

## Effect of Heat Treatment on the Tensile Behavior of 17-4 PH Stainless Steel Additively Manufactured by Metal Binder Jetting

P.D. Nezhadfar<sup>1,2</sup>, Benoit Verquin<sup>3</sup>, Fabien Lefebvre<sup>3</sup>, Christophe Reynaud<sup>3</sup>, Maxime Robert<sup>3</sup>,  
Nima Shamsaei<sup>1,2</sup>

<sup>1</sup>Department of Mechanical Engineering, Auburn University, Auburn, AL, USA

<sup>2</sup>National Center for Additive Manufacturing Excellence (NCAME),  
Auburn University, Auburn, AL, USA

<sup>3</sup>Cetim, 60304 Senlis, France

\*Corresponding author:

Email: [shamsaei@auburn.edu](mailto:shamsaei@auburn.edu)

Phone: (334) 844 4839

### Abstract

Metal Binder Jetting (MBJ), a non-fusion-based powder bed additive manufacturing (AM) process, enables the fabrication of complex geometries with minimum residual stresses. Various materials have been successfully manufactured via the MBJ process; however, appropriate post-process heat treatments are required to enhance their mechanical performance as compared to the wrought or other additively manufactured counterparts. This study aims to investigate the effect of post-manufacture heat treatment on the microstructure and mechanical properties of MBJ 17-4 PH stainless steel (SS). Various heat treatment procedures following the standard routes for the wrought 17-4 PH SS are conducted to evaluate their effects on the tensile behavior of MBJ 17-4 PH SS. The mechanical behavior of the MBJ 17-4 PH SS in various heat treatment conditions is discussed based on their corresponding microstructure.

*Keywords:* Metal binder jetting (MBJ); Stainless steel; Microstructure; Heat treatment; Tensile

### Introduction

Metal binder jetting (MBJ) is categorized as a multi-step additive manufacturing (AM) process following ISO/ASTM52900-15 [1]. However, contrary to the laser-based powder bed AM processes, MBJ is a non-fusion AM technique. In this technique, the spread powder is selectively joined with typically a polymeric binder, layer-by-layer until the desired part geometry is formed in a box of powder. The parts are further consolidated by several stages as follows and shown in **Figure 1:**

- Curing or drying: the box produced (green parts and powder together) is placed in the oven to dry the ink. This will allow the green parts to harden -thanks to binder crosslinking reaction- to be recovered and handled.
- Powder removal: during which the non-amalgamated powder is extracted from the box in order to recover the parts. Moving the parts at this stage may be difficult because they are in green condition. The powder is further recovered and recycled.

- Debinding: this operation consists of removing organic binder from the part by using evaporation and decomposition mechanisms and leaving only a metal part with high porosity of about 35-40 %.
- Sintering: it gives the part its final shape. The part is heated to 80-90 % of the melting temperature of the material to sinter and coalesce the powder particles. Porosity is reduced, and the density is increased due to a fairly uniform shrinkage fairly about 14-16 % (following the definition of shrinkage with sintering indicated in ISO 4492), so that the part proportions are maintained.

The MBJ technique is compatible with any powder material in contrast to other fusion-based AM techniques (e.g., laser beam powder bed fusion (LB-PBF), laser beam directed energy deposition (LB-DED), laser-foil-printing (LFP) [2], etc.). Since the fabrication of the part via MBJ is at a low temperature (typically  $\approx 80^{\circ}\text{C}$  in our case), there are no such issues as oxidation, and residual stress, and the powder surrounding the part in the box is highly recyclable. No support structure is needed for the MBJ parts in contrast to fusion-based techniques. However, depending on the shape of the part, a sintering setter may be needed; this setter that is printed at the same time as the part is not physically connected to it as the support structure for the LB-PBF. The setter is used to prevent any part walls collapsing where there are overhangs or to support compacting of the material during sintering in order to prevent any unwanted deformations.

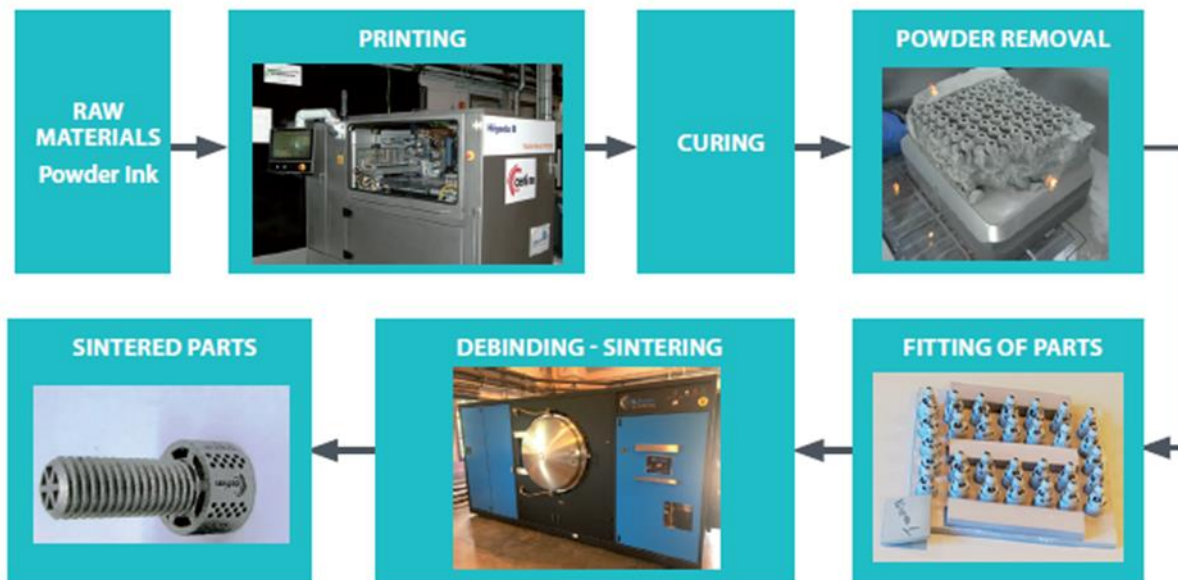


**Figure 1.** Typical Metal Binder Jetting (MBJ) process cycle [3].

There are drawbacks to the MBJ technique; it is a multi-step process to finish a part ready to be deployed in any application, as-sintered parts usually have densities around (97-98%), which is lower than that of LB-PBF specimens but with the same range as Metal Injection Molding ones. Due to the substantial shrinkage during sintering, the main challenge in MBJ would be controlling the size and the mass of parts. Difficulty in controlling the tolerances for the size and mass of the parts increases with component size. The larger the part is, the more difficult it will be to maintain tight tolerances and avoid cracking during sintering.

Various material systems such as nickel-based superalloys [4–6], titanium alloys [7,8], and iron and stainless steels [9] have been manufactured via the MBJ process, and efforts have been made to optimize the sintering temperature and post heat treatment processes for different materials. Mostafaei et al. [5] optimized the sintering and post process heat treatment for the MBJ Inconel 625 to be comparable to the conventionally manufactured counterparts. Similarly, Karlsson et al. [10] studied the post heat treatment effects on the mechanical properties of MBJ AlCoCrFeNi high entropy alloy and reported superior mechanical strength and ductility as compared to those of Inconel 625 and Inconel 718 alloys.

One of the prominent materials used in the AM industry is 17-4 PH stainless steel. This material possesses a desirable combination of strength, ductility, fatigue strength, and high corrosion resistance, which finds use in key engineering, defense, and energy sectors. Therefore, there has been a strong desire to adopt 17-4 PH SS for AM to take advantage of its benefits [11]. The 17-4 PH SS has been successfully manufactured via various laser-based AM techniques. There have been several studies that investigated the effect of powder recycling [12,13], shielding gas type [11,14], build orientation [15,16], surface roughness, and heat treatment [17] on the microstructure and mechanical properties (tensile and fatigue) of LB-PBF 17-4 PH SS.

The main challenge with the AM 17-4 PH SS is to find the most appropriate heat treatment process to enhance its mechanical properties considering the detrimental impacts of induced defects by AM processes. It has been shown that although the peak-age heat treatment (CA-H900) increases the tensile strength of LB-PBF 17-4 PH SS, the fatigue performance is deteriorated after applying this heat treatment [18]. This is attributed to the presence of defects induced by AM process, which makes the high strength material more sensitive in crack initiation and fatigue failure. Nezhadfar et al. [17] investigated the effect of various heat treatment procedures on the microstructure and mechanical properties (tensile and fatigue) of LB-PBF 17-4 PH SS. They reported the CA-H1025 heat treatment procedure as an appropriate heat treatment results in a good combination of tensile strength, ductility, and fatigue performance.

To the best of the authors' knowledge, there is not much literature found on MBJ 17-4 PH SS. This study aims to investigate the effect of various heat treatments on the microstructure and mechanical properties of MBJ 17-4 PH SS. Different heat treatment procedures are applied on the MBJ 17-4 PH SS specimens. The effect of solution heat treatment and aging temperature and duration is studied on the microstructure of MBJ 17-4 PH SS specimens. Eventually, the tensile properties are obtained for each and every one of the applied heat treatments, and the results are discussed according to their corresponding microstructure.

### **Experimental Procedures**

The specimens in this study were fabricated using 17-4 PH SS powder with a particle-size distribution  $D_{10}=7\ \mu\text{m}$ ,  $D_{50} = 14\ \mu\text{m}$ ,  $D_{90} = 23\ \mu\text{m}$ . The chemical composition is listed in **Table 1**.

**Table 1.** Chemical composition of 17-4 PH SS powder used for fabricating the MBJ specimens.

	<b>C</b>	<b>Cr</b>	<b>Ni</b>	<b>Cu</b>	<b>Mn</b>	<b>Si</b>	<b>Nb</b>	<b>Fe</b>
<b>(Wt. %)</b>	0.05	16.00	4.50	4.40	0.30	0.70	0.24	Bal.

The specimens were printed on a Digital Metal Machine DMP2000 with the following process parameters.

- Layer thickness: 42 $\mu$ m, the powder is spread in the Y direction
- Build strategy: “Lissel-4PH” from Digital Metal, with a printing direction in X-axis
- Build orientation of the specimens in the box: X-axis
- Cure time and duration: the box is cured at 205 $^{\circ}$ C for 36 hours

The build layout is shown in **Figure 2** including the cubic coupons (10x10x10 mm<sup>3</sup>) for microstructure characterization and cylindrical bars (diameter of 12 mm, length of 80 mm), which were further machined to tensile test specimens. The green parts were gone through an air debinding cycle of soaking at 345  $^{\circ}$ C for 2 hours after powder removal. The sintering cycle was further conducted on the specimens using an Elnik MIM3015 T furnace under pure hydrogen at 1380  $^{\circ}$ C for 2 hours. After the sintering process, the specimens were undergone hot isostatic pressing (HIP) at 1160  $^{\circ}$ C for 3 hours at a pressure of 1020 bars. The porosity of the HIPed specimens was measured via image analysis to be 0.01%.

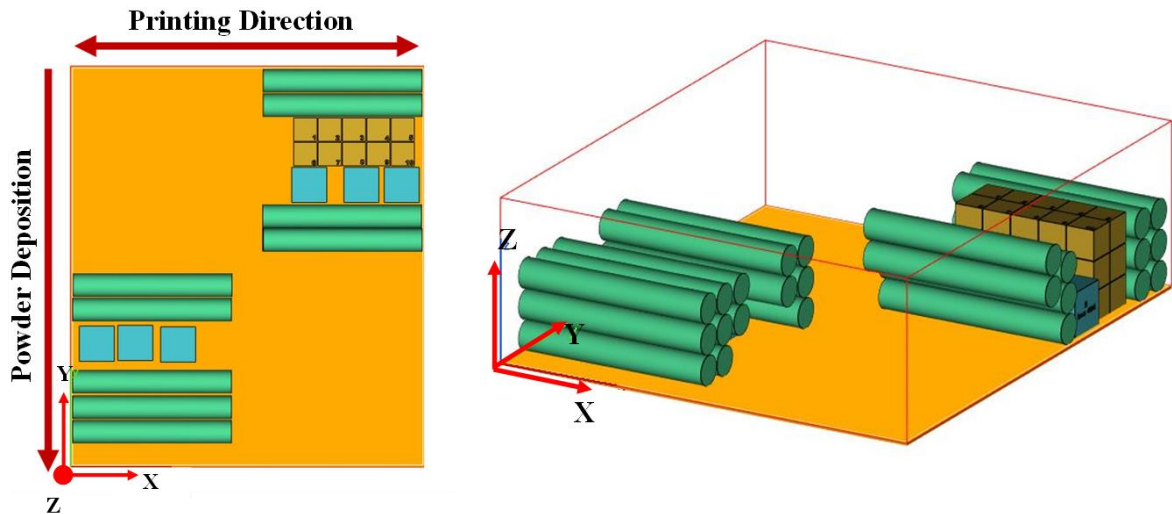


**Figure 2.** Build layout for fabricating MBI 17-4 PH SS specimens.

Cubic coupons shown in **Figure 3** were fabricated for microstructure investigation (see **Figure 2** as well). The cube coupons were cut transversely to characterize the microstructure in XY-plane (i.e., perpendicular to the build direction and parallel to the loading direction seen in **Figure 3(b)**). Specimens were polished using sandpapers with 320-4000 grits, and then mirror-finished using a Chemo-met pad along with using 0.05  $\mu$ m colloidal silica suspension. The specimens were further polished using a vibratory polisher with 0.02  $\mu$ m colloidal silica suspension for 2 hours prior to conducting any microstructure analysis. A Zeiss 550 Crossbeam scanning electron microscope (SEM) with an Oxford electron backscatter diffraction (EBSD) detector was used for microstructure characterization.

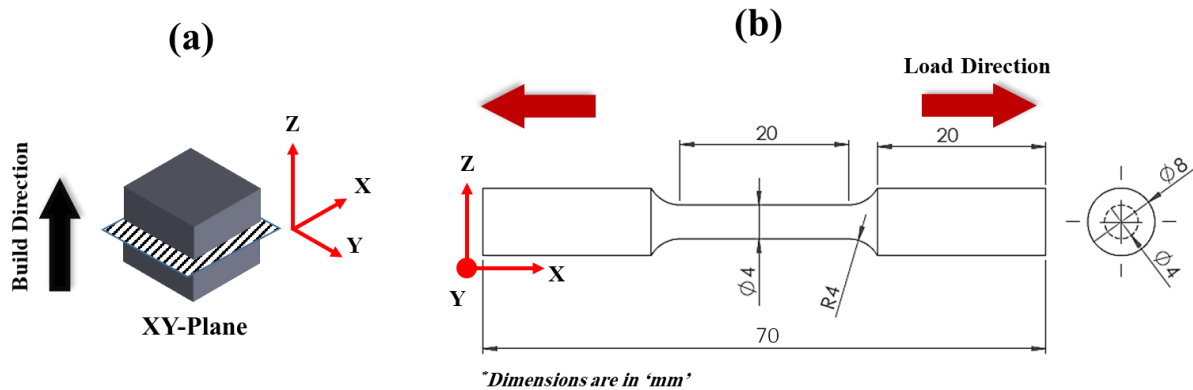


**Figure 3.** (a) The cube coupon for microstructure characterization (XY-plane parallel to load direction was characterized), and (b) the tensile geometry following ASTM E8.

Horizontal cylindrical bars with 10 mm diameter and 67 mm length were fabricated via the MBJ process to be machined into the tensile specimens with the geometry following the ASTM E8 as shown in **Figure 3(b)**. The specimens were heat treated in an argon-purged box furnace following the procedures listed in **Table 2**. The heat treatment procedures are following the ASTM A693 standard [19]; however, in some cases, the solution heat treatment and aging steps were modified to evaluate new heat treatment procedures for this material. The tensile tests were further carried out at a  $0.001 \text{ s}^{-1}$  strain rate to evaluate the mechanical properties of the MBJ 17-4 PH SS specimens in various heat treatment conditions.

**Table 2.** Heat treatment procedures applied on the HIPed MBJ 17-4 PH SS specimens.

Heat Treatment (HT)	Procedure
HT1 (CA-H900)	1050 °C/0.5 hour/Air cooled → 482 °C/1 hour/Air cooled
HT2 (Mod* CA-H900)	1100 °C/1 hour/Air cooled → 482 °C/1 hour/Air cooled
HT3 (Mod1 CA-H1025)	1100 °C/1 hour/Air cooled → 552 °C/0.5 hour/Air cooled
HT4 (Mod2 CA-H1025)	1100 °C/1 hour/Water cooled → 552 °C/0.5 hour/Air cooled

\*Mod = Modified

## **Results and Discussion**

The microstructure characterization results for the as-sintered and HIPed conditions obtained by EBSD are presented in **Figure 4(a)** and (b), respectively. As seen in **Figure 4(a)**, sintering was achieved successfully and parts were fabricated with an adequate density. However, there are still huge pores remained in the microstructure. In addition, the grain boundaries misorientation reveals a high fraction (~67%) of low angle grain boundaries (i.e.,  $5^{\circ}$ - $15^{\circ}$ ). This shows that the grain structure has not developed completely and further post-process thermal treatments are required. The microstructure in the as-sintered condition consists of a martensitic matrix with the presence of coarse strings of  $\delta$ -ferrite with sharp edges.

It can be observed in **Figure 4(b)** that conducting the HIP cycle closes the pores and results in an approximately full dense structure. The microstructure still consists of martensite along with  $\delta$ -ferrite. However, HIP makes most of the  $\delta$ -ferrite grains finer and thinner strings. Moreover, a

higher fraction of high-angle grain boundaries is formed after performing HIP as compared to the as-sintered condition, which witnesses the occurrence of recrystallization of the grain during HIP. Although the HIP process is performed in the austenitic region, there is  $\delta$ -ferrite phase retained in the microstructure. This may be due to the chemical composition of the powder used for fabrication as well as considering the low cooling/heating rates and low solidification rate during the sintering of the parts. Some  $\delta$ -ferrite may be formed during heating above the 1280 °C up to 1380 °C (i.e., the sintering temperature), and also some liquid phase will form during sintering which the low solidification rate results in solidification in the order of liquid  $\rightarrow$   $\delta$ -ferrite+austenite  $\rightarrow$   $\delta$ -ferrite+martensite [20]. The  $\delta$ -ferrite retained in the microstructure from the sintering process will remain in the structure even by performing high temperature heat treatment; however, the morphology of the grains may be changed from sharp edge string-like grains to more circular grains.

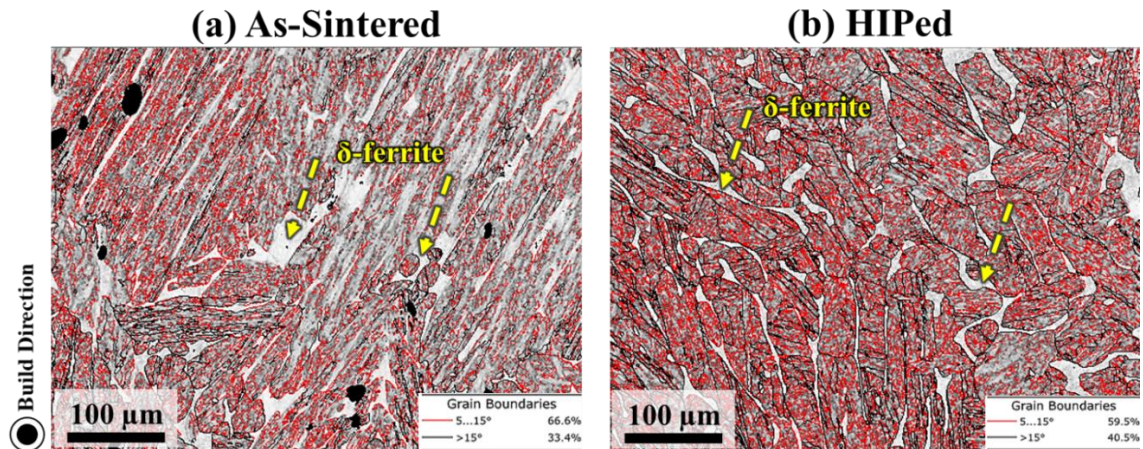


**Figure 4.** EBSD image quality (IQ) juxtaposed by grain boundaries (GB) showing the microstructure of MBJ 17-4 PH SS in (a) as-sintered, and (b) HIPed conditions.

The microstructure of MBJ 17-4 PH SS after different heat treatments (see **Table 2**) is presented in **Figure 5**. An overall observation of the microstructures indicates the martensitic microstructure along with the distributed  $\delta$ -ferrite phase in the microstructure. As was mentioned, even performing solution heat treatment at the austenite region could not resolve the  $\delta$ -ferrite in the microstructure; however, the morphology and the grain sizes varied according to the applied heat treatment. **Figure 5(a)** shows the microstructure of MBJ 17-4 PH SS specimen after HT1 (see **Table 2**) including the martensite and  $\delta$ -ferrite grains. As seen, conducting solution heat treatment at 1050 °C for 0.5 hours could slightly re-arrange the  $\delta$ -ferrite grains as compared to the HIP condition (see **Figure 4**); the  $\delta$ -ferrite grains after heat treatment broken apart and are not as continuous as the ones in the HIP microstructure. However, there are still stretched string-like  $\delta$ -ferrite grains in the microstructure.

Increasing the solution heat treatment temperature from 1050 °C/0.5 hr to 1100 °C/1 hr with the same following aging procedure (i.e., 482 °C/1 hr) in HT2 could break the  $\delta$ -ferrite grains to smaller and more circular ones seen in **Figure 5(b)**. Higher solution heat treatment temperature for a longer duration can result in more fraction of recrystallized austenite grains and result in the re-arrangement of  $\delta$ -ferrite grains in the microstructure. As a result of a higher degree of recrystallization in the microstructure can be referred to the higher high angle grain boundaries in HT2 condition as compared to the HT1.

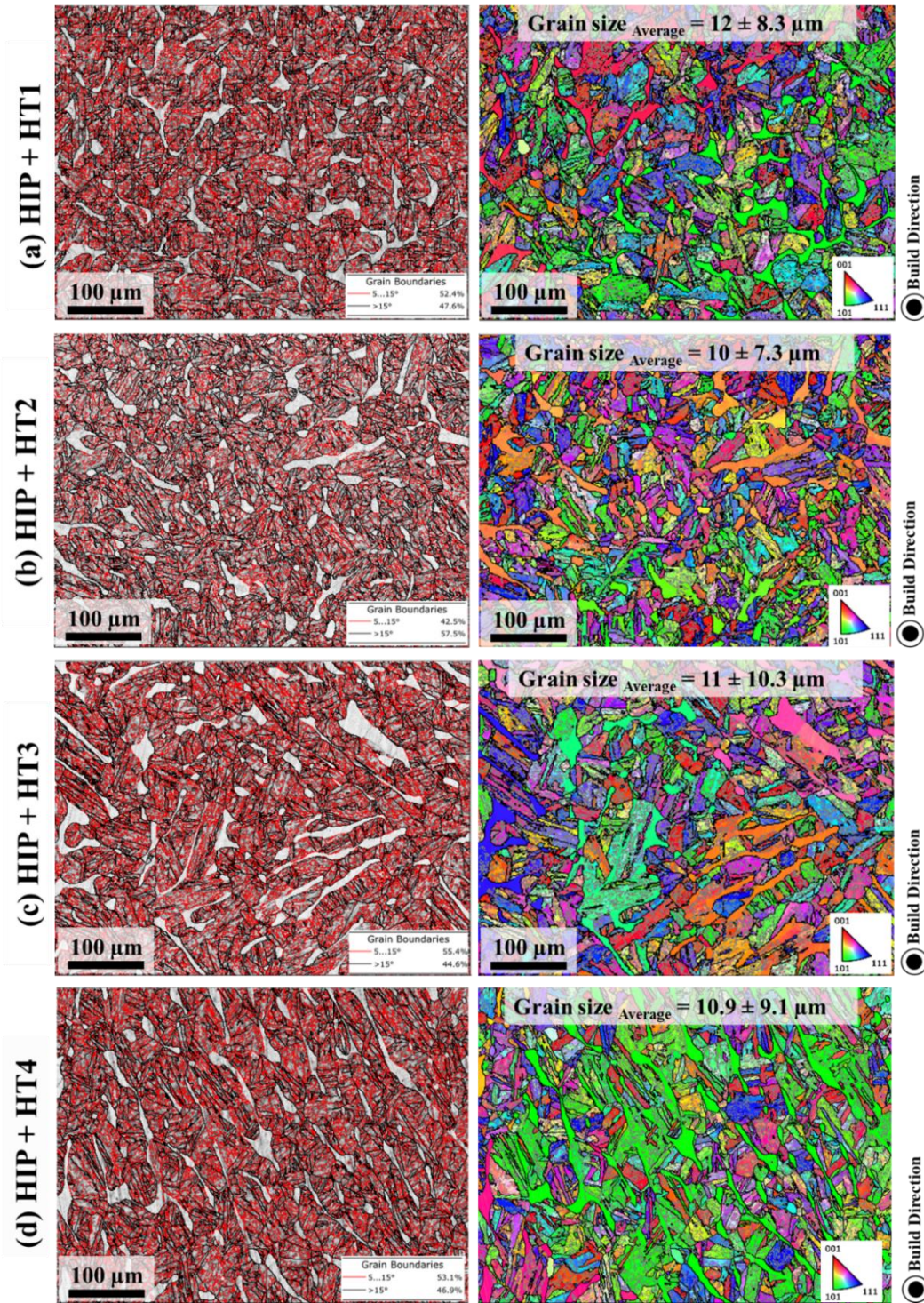


**Figure 5.** EBSD IQ+GB and inverse pole figure (IPF) maps of MBI 17-4 PH SS for: (a) HIP+HT1, (b) HIP+HT2, (c) HIP+HT3, and (d) HIP+HT4 specimens.

It can be observed for the HT3 condition shown in **Figure 5(c)** that at the constant solution heat treatment temperature and duration (i.e., 1100 °C/ 1 hour) as that of HT2, increasing the aging temperature to 552 °C can result in a slight growth of  $\delta$ -ferrite phase, and higher low angle grain boundaries as compared to the HT2 condition. Higher fraction of low angle boundaries is due to

the high temperature aging; however, not sufficient time for the rearrangement of dislocations to form high angle grain boundaries [21]. In the HT4 procedure, specimens were quenched in water after solution heat treatment with the same temperatures to investigate the effect of quenching media on the microstructure and mechanical properties as compared to the HT3 condition. It can be observed in **Figure 5(d)** that the grain structure is not changed considerably as compared to the HT3 counterpart; however, due to rapid cooling, the  $\delta$ -ferrite grains are thinner than the HT2 condition, which is ascribed to finer lath martensite in the microstructure of HT4 as compared to HT3.

Tensile properties of the MBJ 17-4 PH SS specimens are presented in **Figure 6**. As seen, the as-sintered specimen has very low ductility due to the presence of large pores (see **Figure 4(a)**). However, the ductility of the material increases significantly after performing HIP ascribed to the closure of the pores (see **Figure 4(b)**), which enhances the structural integrity of the material. Although HIP increases the ductility of the material, it does not change the strength of the material and the tensile strength (i.e.,  $S_y$  and  $S_u$ ) are comparable with that of the as-sintered specimen. A similar observation has been reported for the LB-PBF 316L SS in which the reduction in the porosity by preheating the build platform increases the ductility without any impact on the strength of the material [22]. Conducting the heat treatment after HIP, however, influences both the strength and ductility of the MBJ 17-4 PH SS specimen. HT1 increases the tensile strength and reduces the ductility as compared to the HIP condition, yet possesses higher ductility than as-sintered specimen. The high strength in the HT1 specimen is attributed to the formation of nano-size Cu-enriched precipitates in the microstructure [23]. Considering the presence of the  $\delta$ -ferrite phase, known as a brittle phase with the limited active slip systems during deformation [24], the MBJ 17-4 PH SS specimen shows a brittle behavior result in relatively low ductility.

The presence of  $\delta$ -ferrite retained from the solidification is inevitable in all the heat treatment conditions, however, conducting prior heat treatment may alter its morphology and size. As seen in **Figure 5(b)**, by conducting HT2 with higher solution heat treatment temperature and duration (i.e., 1100 °C/1hr) as compared to that of HT1 (i.e., 1050 °C/0.5hr), the  $\delta$ -ferrite grains are broken apart and become more circular with less sharp edges compared to those in HT1 condition. This change in the morphology of the brittle  $\delta$ -ferrite phase by applying HT2 makes the material less brittle and enhances the ductility of the material compared to the HT1 specimen as confirmed in **Figure 6**.

Furthermore, at a constant solution heat treatment temperature as HT2, increasing the aging temperature to higher temperature and shorter duration (i.e., 552 °C/0.5 hr) in HT3, the ductility of the material increases considerably, and the strength decreases. It can be seen in **Figure 5(c)** that although most  $\delta$ -ferrite grains have more curved edges, the grain growth occurred due to the higher aging duration, which can be the reason for the reduction in strength of the material. At the same time, it is expected that the ductility decreases due to the presence of larger  $\delta$ -ferrite grains in the microstructure. However, since HT3 is an averaging heat treatment condition, it is reported that the Cu-enriched precipitates are coarsened and semi-coherent with the matrix. In this case, dislocations cannot shear the precipitates and must loop around and bypass the precipitates following the Orowan mechanism [25], which results in higher ductility as compared to the HT2 condition. It has been well established that conducting overage heat treatment on the AM 17-4 PH SS decreases the strength and increases the ductility to some extent [17].

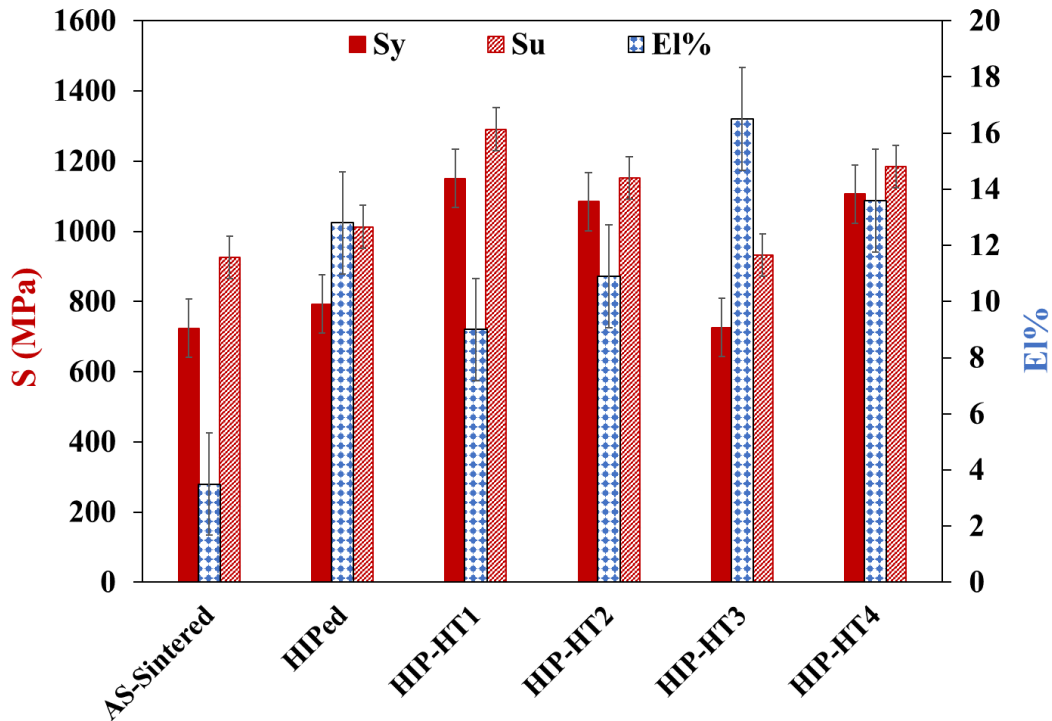


**Figure 6.** Tensile properties (i.e.,  $S_y$ ,  $S_u$ , and  $El\%$ ) of MBJ 17-4 PH SS specimens in various conditions. The standard deviation is shown by error bars.

According to the effect of morphology and size of  $\delta$ -ferrite phase, as well as the size of the Cu-enriched precipitates on strength and ductility, a heat treatment is required to result in preferably small and more circular  $\delta$ -ferrite phase, or at least with curved edges, as well as not coarsened Cu-enriched precipitates. This combination may enhance the strength as compared to the HT3 condition without sacrificing much ductility. As seen, changing the quenching media from air to water in the HT4 condition increases the strength and slightly decreases the ductility as compared to the HT3 condition. Interestingly enough, the strength obtained by HT4 is comparable with that of HT2, slightly lower than that of HT1, yet the ductility of the HT4 specimen is higher than that of both HT2 and HT1 specimens.

### Conclusions

In this study, the effect of heat treatment on the microstructure and tensile properties of MBJ 17-4 PH SS was investigated. The microstructure of MBJ 17-4 PH SS specimens was characterized in the as-sintered condition and after HIP as the reference. Further, various heat treatment conditions with different solution heat treatment and aging temperatures and duration, as well as different quenching media were applied to obtain acceptable strength and ductility for the MBJ 17-4 PH SS. The following conclusions are drawn based on the experimental results:

1. There were large pores and a high fraction of low angle grain boundaries remained in the microstructure of the as-sintered specimen, which the HIP process successfully closed all the pores and developed the grain structure having a higher fraction of high angle grain boundaries. This was attributed to the occurrence of grain recrystallization.

2. The strings of  $\delta$ -ferrite phase with sharp edges retained in the microstructure of as fabricated MBJ 17-4 PH SS specimens, which was attributed to the chemical composition of material as well as low cooling/heating rates and the low solidification rate of MBJ process after sintering in a very high temperature in which the  $\delta$ -ferrite was formed.
3. Conducting well-known peak age heat treatment (i.e., CA-H900) called HT1 herein, increased the strength considerably, while it decreased the ductility. This was attributed to the formation of nano-size Cu-enriched precipitates.
4. Increasing the solution heat treatment temperature and duration (e.g., HT2 vs. HT1) broke the  $\delta$ -ferrite phases apart to more circular in shape with more curvature in edges. This was found to enhance the ductility of the material.
5. Comparable tensile strength (i.e.,  $S_y$ , and  $S_u$ ) and higher ductility than the peak-age condition (i.e., HT1) were obtained by changing the solution heat treatment quenching media to water.

### References

- [1] ISO/ASTM 52900:2015(E), Standard Terminology for Additive Manufacturing – General Principles – Terminology, (n.d.).
- [2] C.-H. Hung, W.-T. Chen, M.H. Sehhat, M.C. Leu, The effect of laser welding modes on mechanical properties and microstructure of 304L stainless steel parts fabricated by laser-foil-printing additive manufacturing, *Int. J. Adv. Manuf. Technol.* 2020 1123. 112 (2020) 867–877. <https://link.springer.com/article/10.1007/s00170-020-06402-7> (accessed August 26, 2021).
- [3] B. Verquin, S. Hognin, C. Reynaud, C. Quentin, *Metal additive manufacturing - The essentials*, 2019.
- [4] M. Turker, D. Godlinski, F. Petzoldt, Effect of production parameters on the properties of IN 718 superalloy by three-dimensional printing, *Mater. Charact.* 59 (2008) 1728–1735.
- [5] A. Mostafaei, Y. Behnamian, Y.L. Krimer, E.L. Stevens, J.L. Luo, M. Chmielus, Effect of solutionizing and aging on the microstructure and mechanical properties of powder bed binder jet printed nickel-based superalloy 625, *Mater. Des.* 111 (2016) 482–491.
- [6] P. Nandwana, A.M. Elliott, D. Siddel, A. Merriman, W.H. Peter, S.S. Babu, Powder bed binder jet 3D printing of Inconel 718: Densification, microstructural evolution and challenges☆, *Curr. Opin. Solid State Mater. Sci.* 21 (2017) 207–218.
- [7] S. Maleksaedi, J.K. Wang, A. El-Hajje, L. Harb, V. Guneta, Z. He, F.E. Wiria, C. Choong, A.J. Ruys, Toward 3D printed bioactive titanium scaffolds with bimodal pore size distribution for bone ingrowth, in: *Procedia CIRP*, Elsevier B.V., 2013: pp. 158–163.
- [8] F.E. Wiria, J.Y.M. Shyan, P.N. Lim, F.G.C. Wen, J.F. Yeo, T. Cao, Printing of Titanium implant prototype, *Mater. Des.* 31 (2010) S101–S105.

- [9] S. Mirzababaei, S. Pasebani, A review on binder jet additive manufacturing of 316L stainless steel, *J. Manuf. Mater. Process.* 3 (2019) 82. [www.mdpi.com/journal/jmmp](http://www.mdpi.com/journal/jmmp) (accessed May 25, 2021).
- [10] D. Karlsson, G. Lindwall, A. Lundbäck, M. Amnebrink, M. Boström, L. Riekehr, M. Schuisky, M. Sahlberg, U. Jansson, Binder jetting of the AlCoCrFeNi alloy, *Addit. Manuf.* 27 (2019) 72–79.
- [11] P.D. Nezhadfar, K. Anderson-Wedge, S.R. Daniewicz, N. Phan, S. Shao, N. Shamsaei, Improved high cycle fatigue performance of additively manufactured 17-4 PH stainless steel via in-process refining micro-/defect-structure, *Addit. Manuf.* 36 (2020) 101604.
- [12] A. Soltani-Tehrani, J. Pegues, N. Shamsaei, Fatigue behavior of additively manufactured 17-4 PH stainless steel: the effects of part location and powder re-use, *Addit. Manuf.* 33 (2020).
- [13] P.D. Nezhadfar, A. Soltani-Tehrani, A. Sterling, N. Tsolas, N. Shamsaei, The effects of powder recycling on the mechanical properties of additively manufactured 17-4 PH stainless steel, in: *Solid Free. Fabr. 2018 Proc. 29th Annu. Int. Solid Free. Fabr. Symp. - An Addit. Manuf. Conf. SFF 2018*, 2020.
- [14] P.D. Nezhadfar, M. Masoomi, S.M. Thompson, N. Phan, N. Shamsaei, Mechanical properties of 17-4 PH stainless steel additively manufactured under Ar and N<sub>2</sub> shielding gas, in: *Proc. 29th Annu. Int. Solid Free. Fabr. Symp. – An Addit. Manuf. Conf.*, Austing, TX, 2018: pp. 1301–1310.
- [15] A. Yadollahi, N. Shamsaei, S.M. Thompson, A. Elwany, L. Bian, Effects of building orientation and heat treatment on fatigue behavior of selective laser melted 17-4 PH stainless steel, *Int. J. Fatigue.* 94 (2017) 218–235.
- [16] P.D. Nezhadfar, E. Burford, K. Anderson-Wedge, B. Zhang, S. Shao, S.R. Daniewicz, N. Shamsaei, Fatigue crack growth behavior of additively manufactured 17-4 PH stainless steel: Effects of build orientation and microstructure, *Int. J. Fatigue.* 123 (2019).
- [17] P.D. Nezhadfar, R. Shrestha, N. Phan, N. Shamsaei, Fatigue behavior of additively manufactured 17-4 PH stainless steel: Synergistic effects of surface roughness and heat treatment, *Int. J. Fatigue.* 124 (2019).
- [18] N. Shamsaei, A. Yadollahi, L. Bian, S.M. Thompson, An overview of Direct Laser Deposition for additive manufacturing; Part II: Mechanical behavior, process parameter optimization and control, *Addit. Manuf.* 8 (2015) 12–35.
- [19] ASTM A693-16, Standard specification for precipitation-hardening stainless and heat-resisting steel plate, sheet, and strip, *ASTM Int.* (2016).
- [20] P. Sathiya, M.K. Mishra, B. Shanmugarajan, Effect of shielding gases on microstructure

and mechanical properties of super austenitic stainless steel by hybrid welding, *Mater. Des.* 33 (2012) 203–212.

- [21] F.J. Humphreys, M. Hatherly, *Recrystallization and related annealing phenomena*, Elsevier, 2004.
- [22] P.D. Nezhadfar, N. Shamsaei, N. Phan, Enhancing ductility and fatigue strength of additively manufactured metallic materials by preheating the build platform, *Fatigue Fract. Eng. Mater. Struct.* 44 (2021) 257–270.
- [23] L.E. Murr, E. Martinez, J. Hernandez, S. Collins, K.N. Amato, S.M. Gaytan, P.W. Shindo, Microstructures and properties of 17-4 PH stainless steel fabricated by Selective Laser melting, *J. Mater. Res. Technol.* 1 (2012) 167–177.
- [24] E. Pereloma, D. Edmonds V, *Phase transformations in steels 2: diffusionless transformations, high strength steels, modelling and advanced analytical techniques*, Woodhead Publishing, 2012.
- [25] G.E. Dieter, *Mechanical Metallurgy*, 3rd ed., McGraw-Hill, Boston, MA, MA, 1986.